Electronic Supplementary Information for:

Modulating the intersystem crossing efficiency of anthracene carboxyimide based photosensitizers via structural adjustment and application as potent photodynamic therapeutic reagent

*Hui Liang [‡ a], Liting Tang [‡ a], Jiaxing He [b], Jianqing Li [c], Zeduan Chen [a], Shuqing Cai [a], Junhong Pang [b], Zafar Mahmood [*a], Wencheng Chen [a], Ming-De Li [*b], Zujin Zhao [*c], Yanping Huo [a], Shaomin Ji [*a]*

[a] School of Chemical Engineering and Light Industry, Guangdong University of Technology, Guangzhou, 510006, PR China

. E-mail: zafarchemistry18@gmail.com, smji@gdut.edu.cn

[b] Department of Chemistry and Key Laboratory for Preparation and Application of Ordered Structural Materials of Guangdong Province, Shantou University, Shantou, 515063, PR China.

E-mail: mdli@stu.edu.cn

[c] State Key Laboratory of Luminescent Materials and Devices, Guangdong Provincial Key Laboratory of Luminescence from Molecular Aggregates, South China University of Technology, Guangzhou 510640, PR China.

E-mail: mszjzhao@scut.edu.cn

[‡]H. L. and L.T.T. contributed equally to this work.

Contents

1. Synthesis of the Compounds

1, 2, Br-ACI were synthesized according to literature methods[1-3].

Synthesis of Br-ACI

2 (400 mg, 1.22 mmol) was dissoved in a flask with 150 mL ethanol, under N_2 atmosphere, reaction mixture was deoxygenated by using a vacuum pump. Then *n*-butylamine (0.12 ml, 1.22 mmol) was injected into the reaction solution, reflux for 12 h under stirring, and then cool to room temperature. After adding silica gel powder, it is evaporated to powder, and purified by silica gel column (*n*-hexane: dichloromethane =3:1). After purification, a yellow solid (160 mg) was obtained with a yield of 34 %. ^{1}H NMR (400 MHz, $CDCl_3$) δ 10.16 (d, *J* = 8.0 Hz, 1H), 8.81 – 8.58 (m, 2H), 8.10 (d, *J* = 8.5 Hz, 2H), 7.78 – 7.67 (m, 1H), 7.47 – 7.36 (m, 3H), 7.31 (m, 7.0 Hz, 1H), 7.21 (d, *J* = 4.0 Hz, 2H), 7.16 – 7.07 (m, 2H), 6.89 (d, *J* = 8.0 Hz, 2H), 4.38 – 4.26 (t, *J* = 8.0 Hz, 2H), 1.80 (m, 2H), 1.47 (m, 7.5 Hz, 2H), 0.98 (t, *J* = 8.0 Hz, 3H). ^{13}C NMR (100 MHz, $CDCl_3$) δ 165.24, 163.88, 147.21, 137.37, 134.27, 133.58, 133.33, 131.32, 130.75, 130.62, 128.62 – 128.30, 128.16, 126.80, 126.22, 125.14, 122.50, 115.30, 40.53, 30.30, 20.55, 13.93. HR-MS *m/z* calculated for $[C_{20}H_{16}BrNO_2+H]^+$=382.04427, found: *m/z* = 382.04369.

Synthesis of Ph-ACI

Under N_2 atmosphere, **Br-ACI** (80 mg, 0.209 mmol), Phenylbornic acid (25 mg, 0.209 mmol), K_2CO_3 (173 mg, 1.25 mmol) was dissolved in toluene / ethanol / water (10 ml / 10 ml / 5 ml), reaction mixture was deoxygenated by using a vacuum pump. Then Pd $(PPh_3)_4$ (12 mg, 5%) was

added and reaction mixture was heated to 90 °C, reflux 8 h under stirring, then cool to room temperature, extract three times with dichloromethane and water, dry with anhydrous sodium sulfate, after evaporation of solvent under reduced pressure, the crude product purification by column chromatography (silica gel, *n*-hexane: dichloromethane =1:1.5), a yellow product (57 mg) was obtained with a yield of 67 %. ^{1}H NMR (400 MHz, $CDCl_3$) δ 10.14 (d, *J* = 12.0 Hz, 1H), 8.77 (m, 1H), 8.00 (d, *J* = 8.0 Hz, 1H), 7.79 (dd, *J* = 8.0 Hz, 2H), 7.67 – 7.55 (m, 4H), 7.53 – 7.45 (m, 1H), 7.44 – 7.36 (m, 2H), 4.36 – 4.25 (m, 2H), 1.89 – 1.74 (m, 2H), 1.51 (m, 2H), 1.02 (t, *J* = 8.0 Hz, 3H). ^{13}C NMR (100 MHz, $CDCl_3$) δ 165.24, 163.88, 147.21, 137.37, 134.27, 133.58, 133.33, 131.32, 130.75, 130.62, 128.62 – 128.30, 128.16, 126.80, 126.22, 125.14, 122.50, 115.30, 40.53, 30.30, 20.55, 13.93. HR-MS *m/z* calculated for $[C_{26}H_{22}NO_2+H]^+$ =380.16505, found: *m/z* = 380.16408.

Synthesis of PY-ACI

Under N_2 atmosphere, **3** (70 mg, 0.18 mmol), **Br-ACI** (68 mg, 0.18 mmol) and K_2CO_3 (74 mg, 0.54 mmol) was dissolved in a flask with 10 ml DMF and 0.5 ml water, reaction mixture was deoxygenated by using a vacuum pump. Then Pd $(PPh_3)_4$ (10 mg, 5%) was added and reaction mixture was heated to 80 ℃ for 4 h under stirring, then cool to room temperature, extract three times with dichloromethane and water, dry with anhydrous sodium sulfate, after evaporation of solvent under reduced pressure, the crude product purification by column chromatography (silica gel, *n*-hexane: dichloromethane =1:1.5), a red product (49 mg) was obtained with a yield of 50 %. ^{1}H NMR (400 MHz, $CDCl_3$) δ 10.12 (d, *J* = 8.0 Hz, 1H), 8.70 (m, 1H), 8.33 (d, *J* = 8.0 Hz, 1H), 8.26 (d, *J* = 8.0 Hz, 1H), 8.15 (dd, *J* = 16.0, 8.0 Hz, 2H), 7.88 (dd, *J* = 8.0, 4.0 Hz, 1H), 7.79 – 7.62 (m, 4H), 7.52 – 7.40 (m, 4H), 7.40 – 7.31 (m, 1H), 7.18 – 7.10 (m, 1H), 6.71 (d, *J* = 8.0 Hz, 1H), 4.36 – 4.21 (t, *J* = 8.0 Hz, 2H), 1.85 – 1.70 (m, 2H), 1.49 – 1.39 (m, 2H), 0.97 (t, *J* = 8.0 Hz, 3H).

^{13}C NMR (100 MHz, $CDCl_3$) δ 164.30, 162.84, 144.60, 133.73, 133.39, 133.13, 132.53, 131.30, 130.99, 130.71, 129.83, 128.55, 127.90, 127.80 – 127.46, 127.31, 126.37, 125.99, 125.85 – 125.48, 125.06, 124.51, 121.73, 119.96 – 119.45, 118.62, 114.73, 39.56, 29.32, 19.54, 12.94. HR-MS *m/z* calculated for $[C_{40}H_{28}NO_2+H]^+$=554.21200, found: *m/z* =554.21185.

Synthesis of NP-ACI

NP-ACI synthesized by following the same method as for **Ph-ACI**. The product was obtained as yellow solid (71 mg, 63%). ^{1}H NMR (400 MHz, $CDCl_3$) δ 10.11 (d, *J* = 12.0 Hz, 1H), 8.69 (d, *J* = 8.0 Hz, 1H), 8.04 (d, *J* = 8.0 Hz, 1H), 7.96 (d, *J* = 8.0 Hz, 1H), 7.80 – 7.67 (m,2H), 7.67 – 7.58 (m, 1H), 7.49 (d, *J* = 8.0 Hz, 1H), 7.46 – 7.37 (m,3H), 7.34 – 7.26 (m, 1H), 7.18 – 7.09 (m, 1H), 6.87 (d, *J* = 8.0 Hz, 1H), 4.36 – 4.18 (t, 2H), 1.82 – 1.70 (m, 2H), 1.50 – 1.40 (m, 2H), 0.97 (t, *J* = 8.0 Hz, 3H). ^{13}C NMR (100 MHz, $CDCl_3$) δ 164.33, 162.89, 144.64, 133.42, 129.86, 127.37, 125.84, 125.12, 121.66, 114.69, 107.55, 39.56, 29.32, 19.54, 12.92. HR-MS *m/z* calculated for $[C_{30}H_{23}NO_2+H]^+$=430.18070, found: *m/z* =430.18010.

Synthesis of AN-ACI

AN-ACI synthesized by following the same method as for **Ph-ACI**. The product was obtained as yellow solid (63 mg, 53%).^{1}H NMR (400 MHz, $CDCl_3$) δ 10.16 (m, 1H), 8.68 (d, *J* = 10.3 Hz, 2H), 8.10 (d, *J* = 8.0 Hz, 2H), 7.81 – 7.66 (m, 1H), 7.39 (m, 3H), 7.36 – 7.25 (m, 1H), 7.21 (d, *J* = 4.0 Hz, 2H), 7.16 – 7.04 (m, 2H), 6.89 (d, *J* = 8.0 Hz, 2H), 4.40 – 4.21 (t, *J* = 8.0 Hz, 2H), 1.80 (m, 2H), 1.51 – 1.40 (m, 2H), 0.98 (t, *J* = 8.0 Hz, 3H). ^{13}C NMR (100 MHz, $CDCl_3$) δ 164.39, 162.84, 143.41, 132.99, 132.51, 131.72, 130.26, 129.98, 128.34, 127.69, 127.26, 126.05, 125.79, 125.56, 125.14, 124.73, 124.53, 121.85, 114.98, 39.58, 29.33, 19.56, 12.94. HR-MS *m/z* calculated for $[C_{34}H_{26}NO_2+H]^+$=480.19635, found: *m/z* =480.19668.

Synthesis of TPA-ACI

TPA-ACI synthesized by following the same method as for **Ph-ACI**. The product was obtained as orange solid (37 mg, 52%).^{1}H NMR (400 MHz, $CDCl_3$) δ 10.15 (d, *J* = 4.0 Hz, 1H), 8.78 (m, 1H), 8.19 (m, 1H), 7.96 (d, *J* = 8.0 Hz, 1H), 7.87 – 7.77 (m, 1H), 7.68 – 7.60 (m, 1H), 7.55 (dd, *J* = 9.8, 6.5 Hz, 1H), 7.36 (m, 4H), 7.30 – 7.23 (m, 8H), 7.15 – 7.05 (m, 2H), 4.40 – 4.24 (t, 2H), 1.81 (m, 2H), 1.51 (m, 2H), 1.02 (t, *J* = 8.0 Hz, 3H). ^{13}C NMR (101 MHz, $CDCl_3$) δ 164.24, 162.90, 147.12, 146.40, 133.47, 132.65, 132.33, 130.54, 129.72, 129.10, 128.51, 127.64, 127.15, 125.80, 125.13, 124.07, 122.65 (s, 6H), 121.50, 121.01, 114.01, 39.49, 29.27, 19.52, 12.91. HR-MS *m/z* calculated for $[C_{38}H_{30}NO_2+H]^+$= 547.23855, found: *m/z* =547.23752.

Synthesis of PY-Ph

PY-Ph synthesized by following the same method as for **Ph-ACI**. The product was obtained as orange solid (45 mg, 58%).^{1}H NMR (400 MHz, $CDCl_3$) δ 8.16 – 8.07 (m, 4H), 7.67 (d, *J* = 8.0 Hz, 1H), 7.60 (d, *J* = 8.0 Hz, 2H), 7.47 – 7.38 (m, 6H), 7.38 – 7.34 (m, 2H), 7.33 (s, 1H). ^{13}C NMR (100 MHz, $CDCl_3$) δ 133.69, 131.94, 130.39, 130.24, 129.62, 128.94, 128.05, 127.65, 127.3, 126.86, 126.60, 126.33, 125.58, 125.47, 125.06, 119.31, 119.08, 118.89. HR-MS *m/z* calculated for $[C_{26}H_{16}NO_2+H]^+$ =329.13303, found: *m/z* =329.13268.

2. Molecular structure characterization data

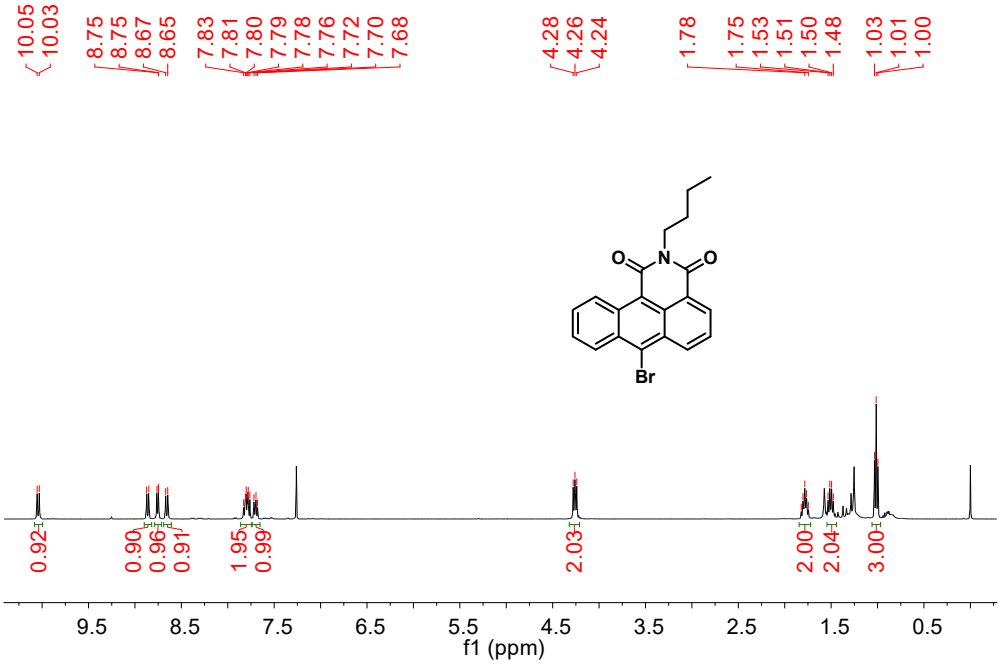

Figure. S1. ^{1}H NMR of **Br-ACI** ($CDCl_3$, 400 MHz).

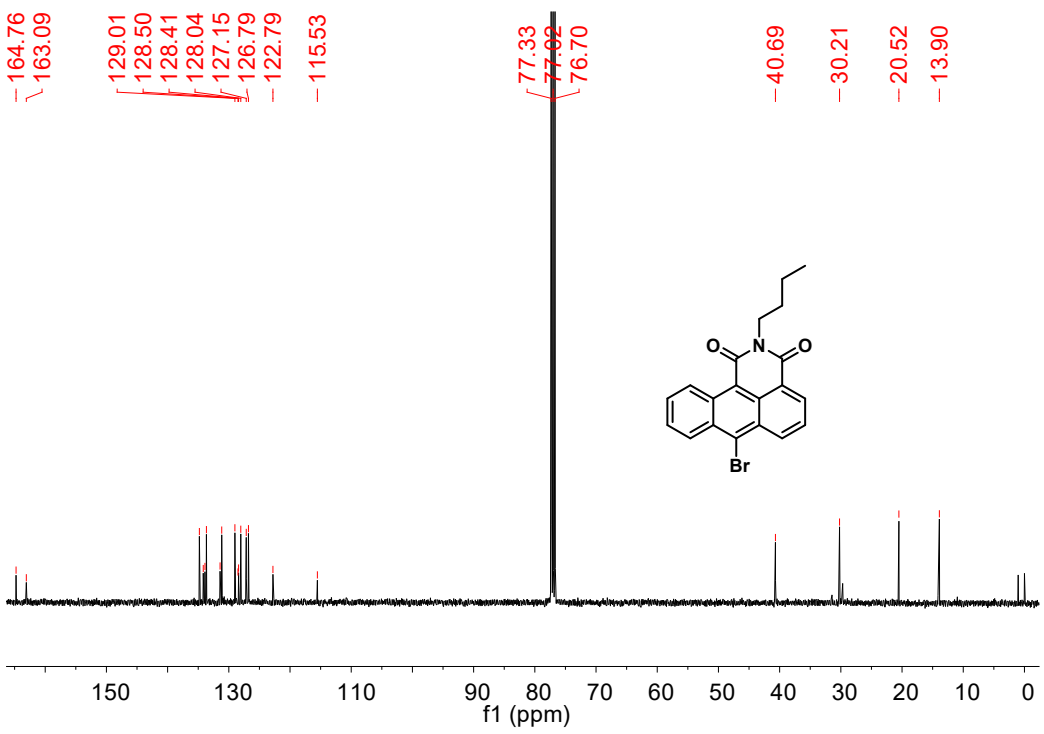

Figure. S2. ^{13}C NMR of **Br-ACI** ($CDCl_3$, 100 MHz).

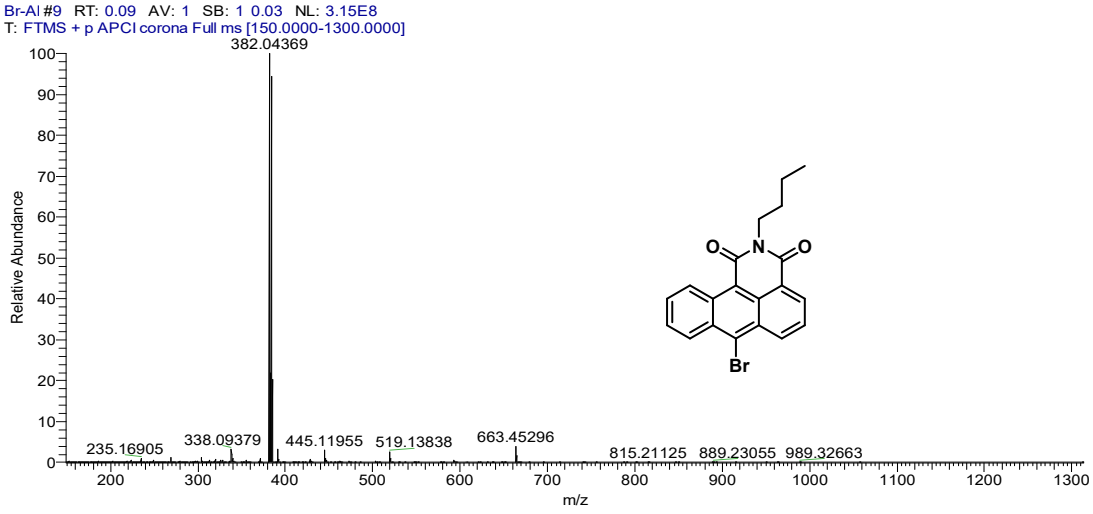

Figure. S3. HRMS of **Br-ACI**.

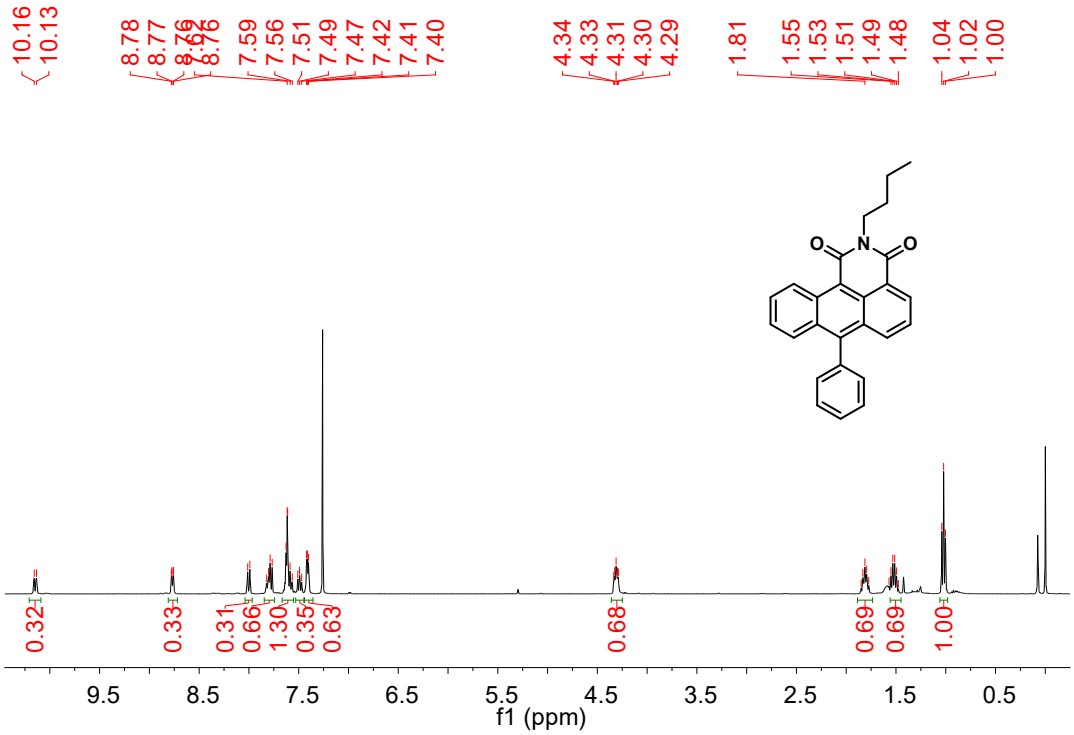

Figure. S4. ^{1}H NMR of **Ph-ACI** ($CDCl_3$, 400 MHz).

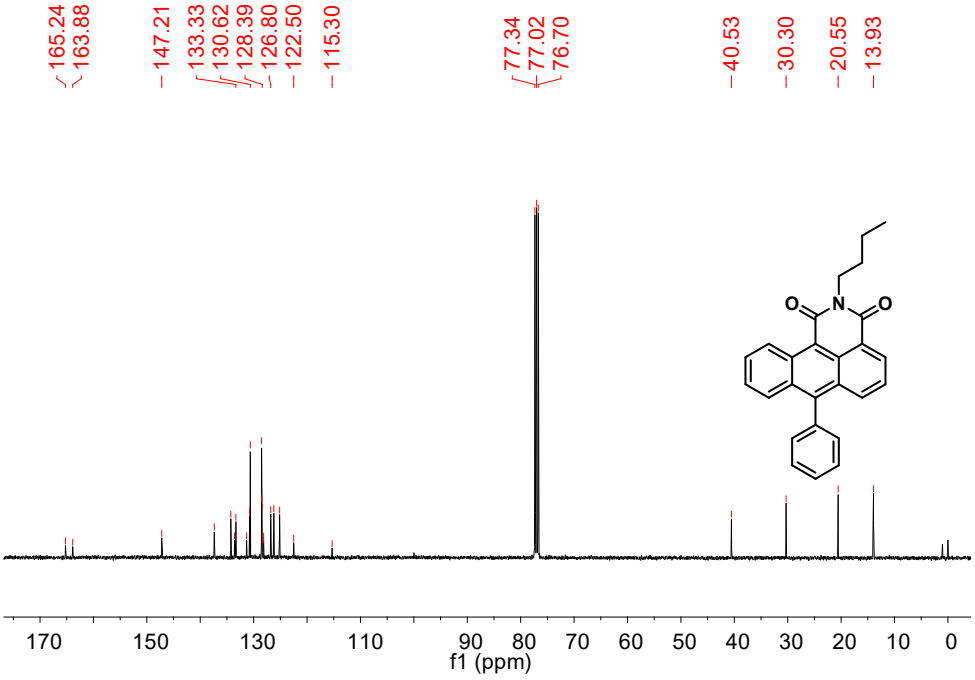

Figure. S5. ^{13}C NMR of **Ph-ACI** ($CDCl_3$, 100 MHz).

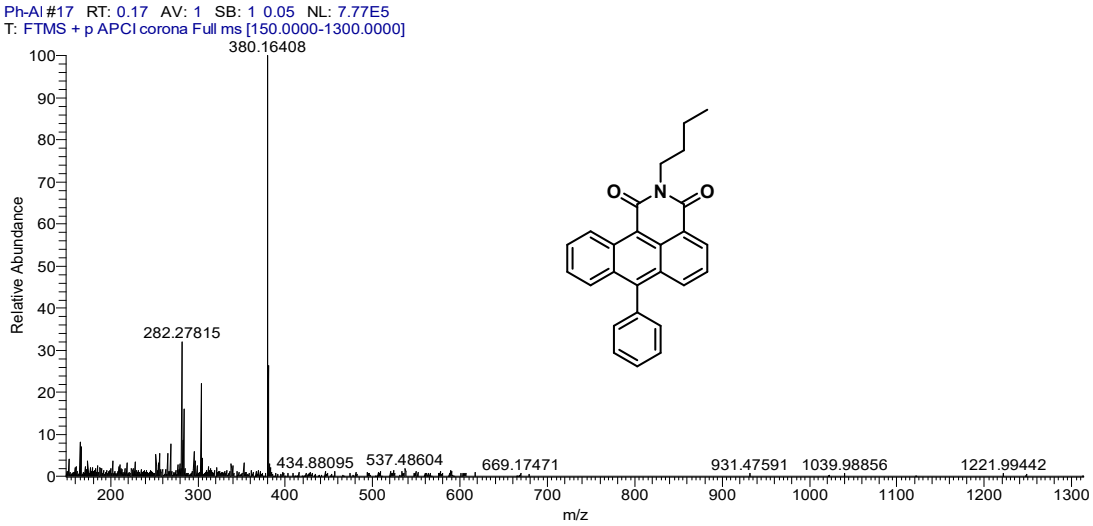

Figure. S6. HRMS of **Ph-ACI**.

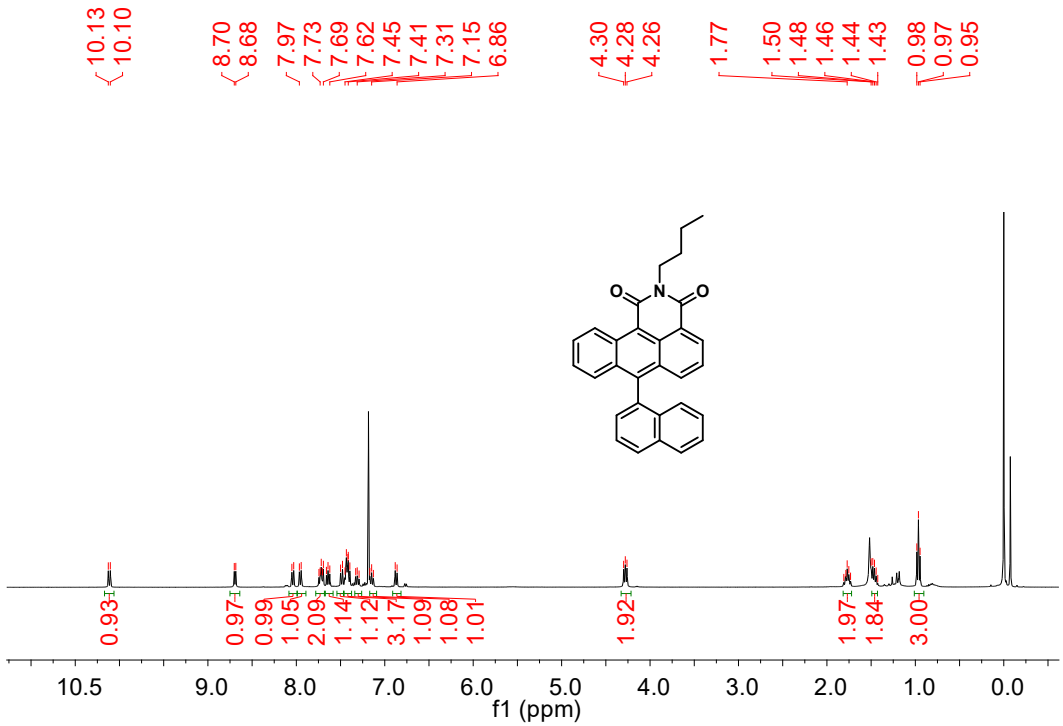

Figure. S7. ^{1}H NMR of **NP-ACI** ($CDCl_3$, 400 MHz).

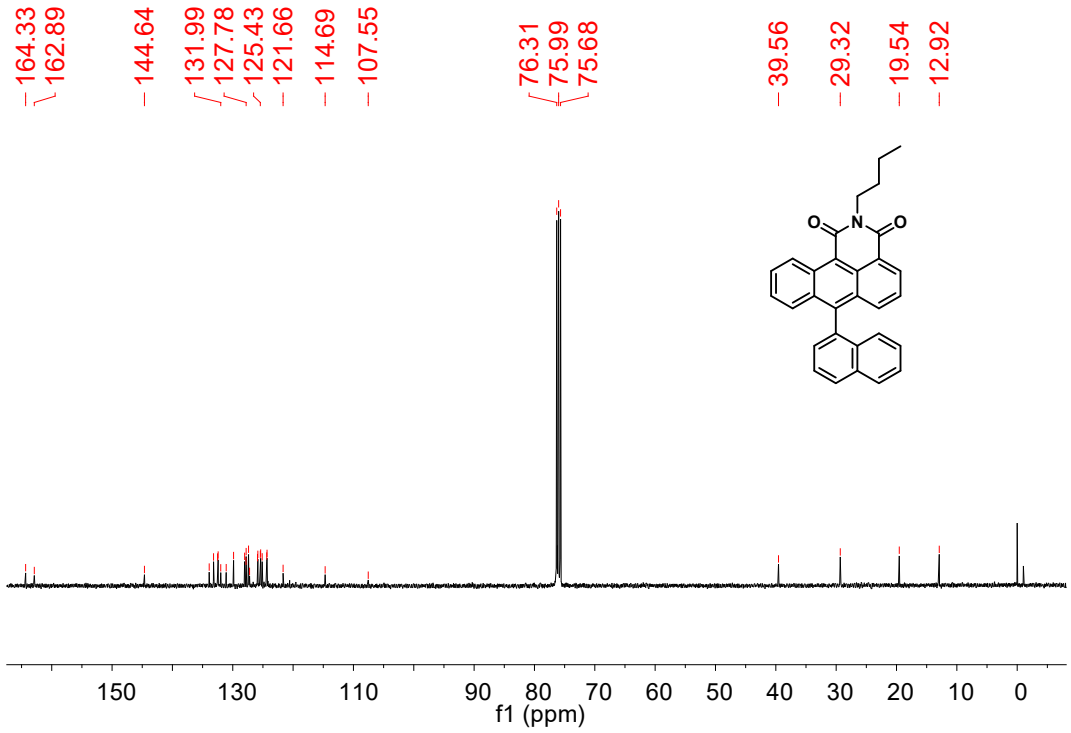

Figure. S8. ^{13}C NMR of **NP-ACI** ($CDCl_3$, 100 MHz).

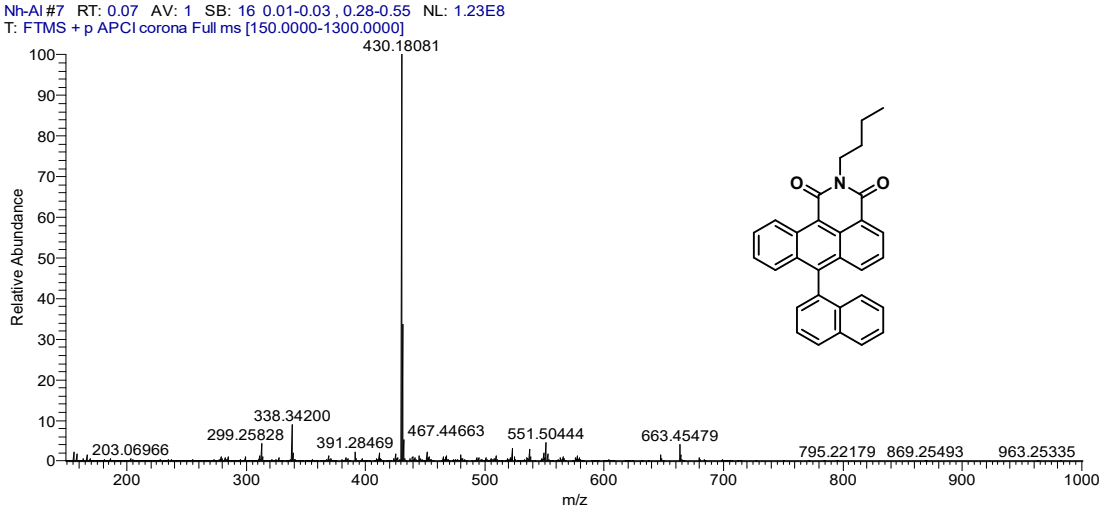

Figure. S9. HRMS of **NP-ACI**.

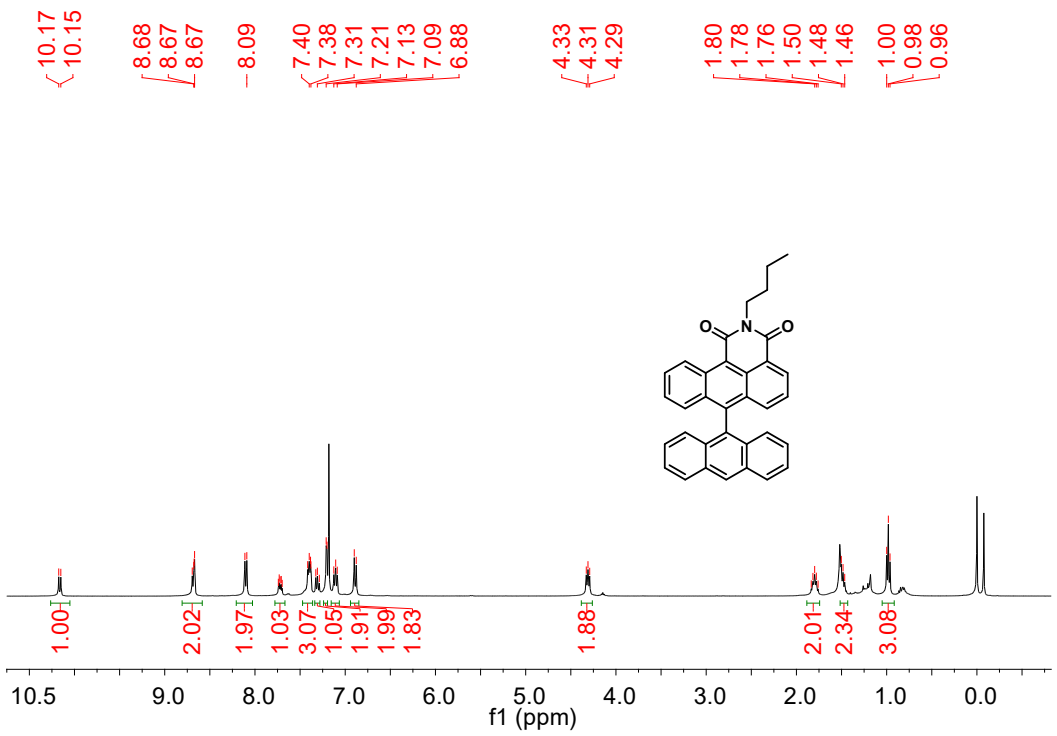

Figure. S10. ^{1}H NMR of **AN-ACI** ($CDCl_3$, 400 MHz).

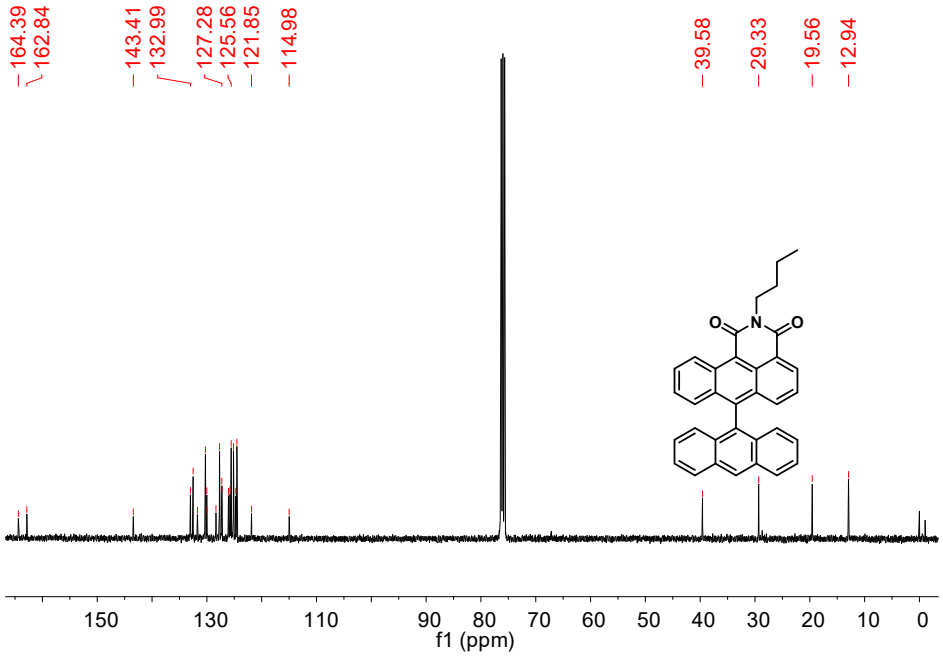

Figure. S11. ^{13}C NMR of **AN-ACI** ($CDCl_3$, 100 MHz).

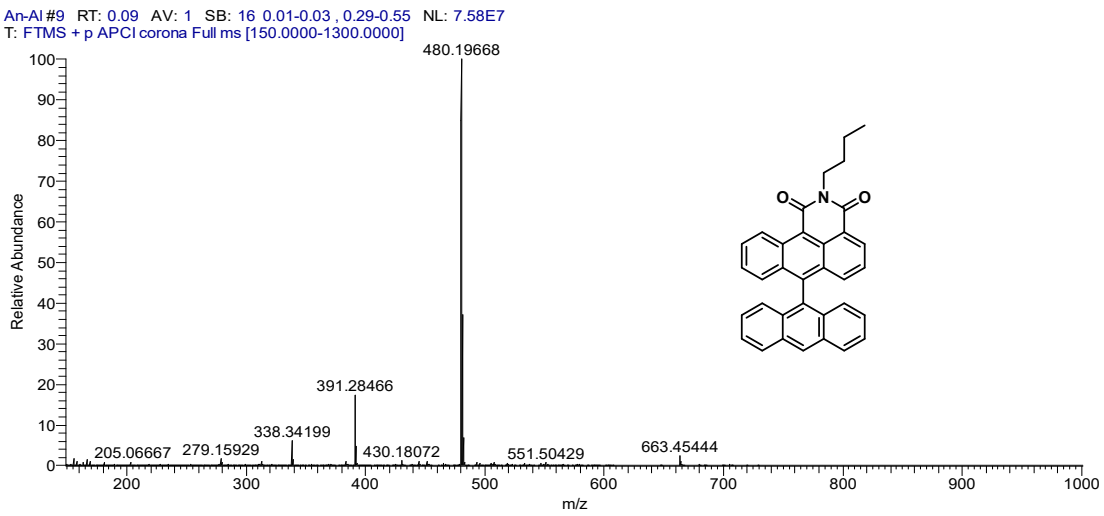

Figure. S12. HRMS of **AN-ACI**.

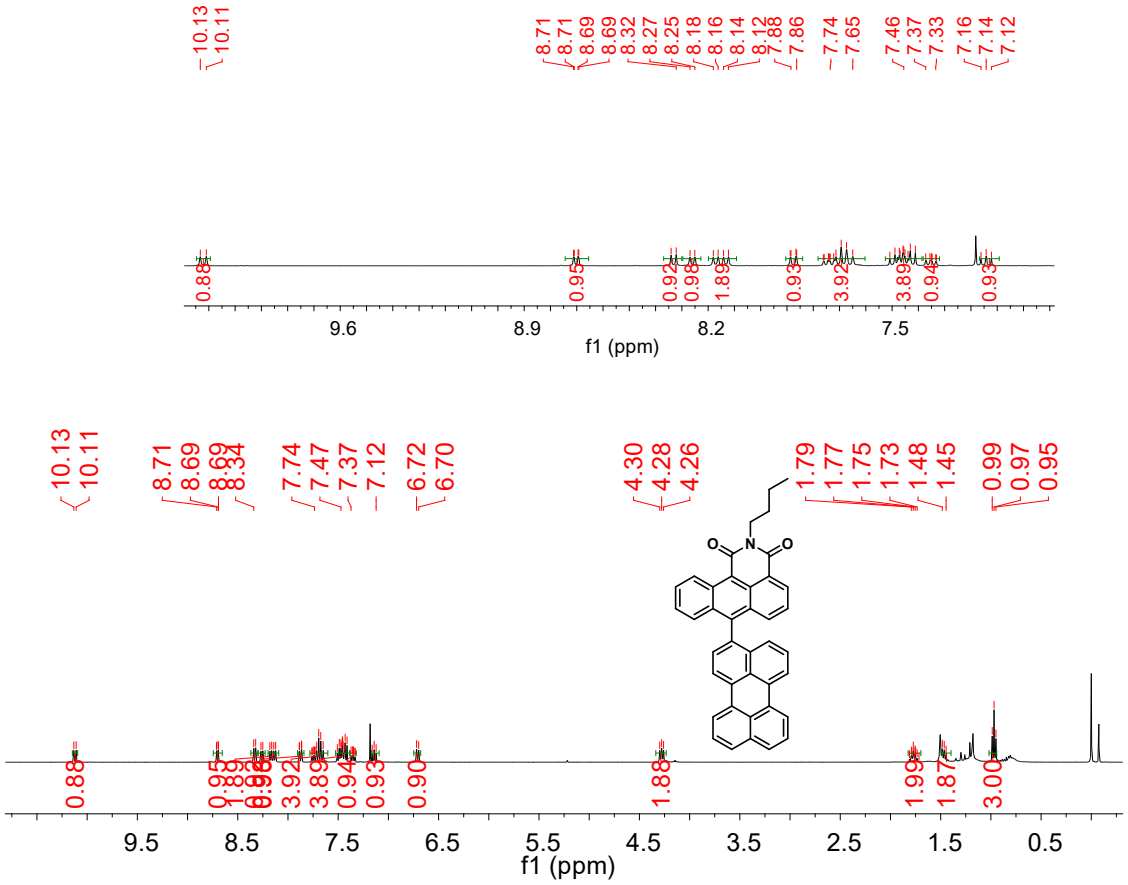

Figure. S13. ^{1}H NMR of **PY-ACI** ($CDCl_3$, 400 MHz).

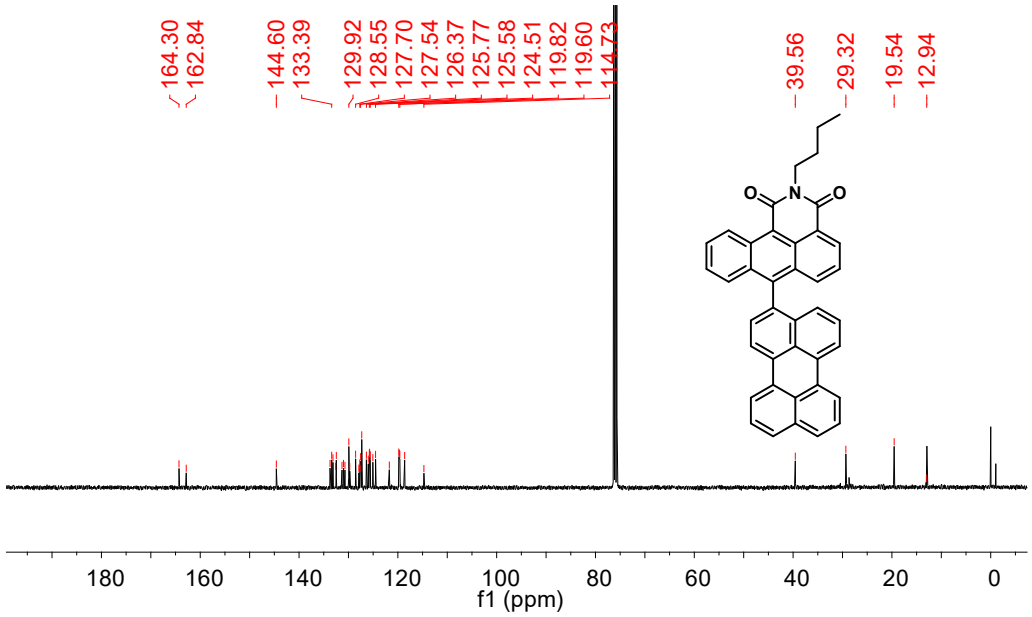

Figure. S14. ^{13}C NMR of **PY-ACI** ($CDCl_3$, 100 MHz).

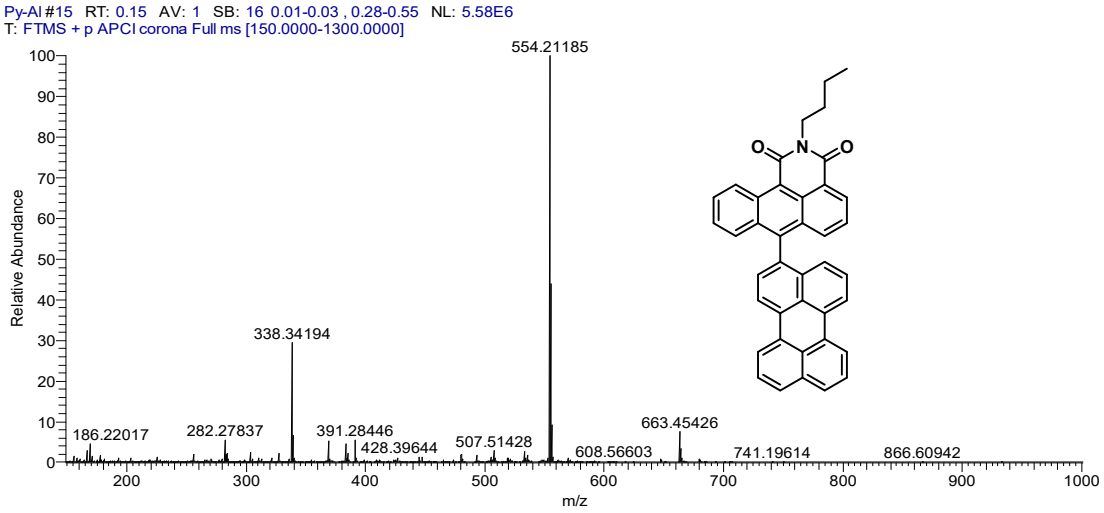

Figure. S15. HRMS of **PY-ACI**.

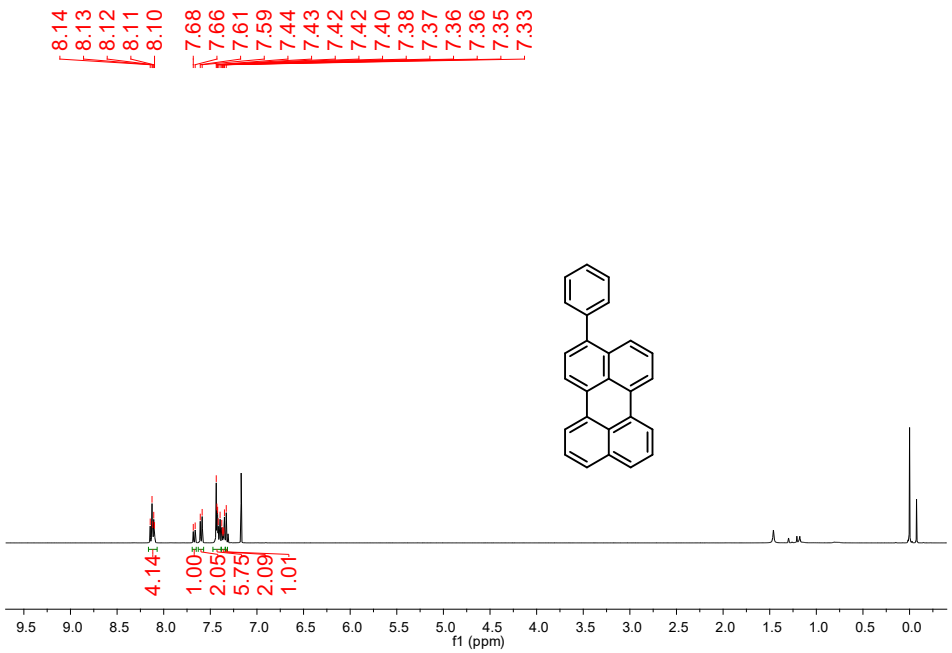

Figure. S16. ^{1}H NMR of **PY-Ph** ($CDCl_3$, 400 MHz).

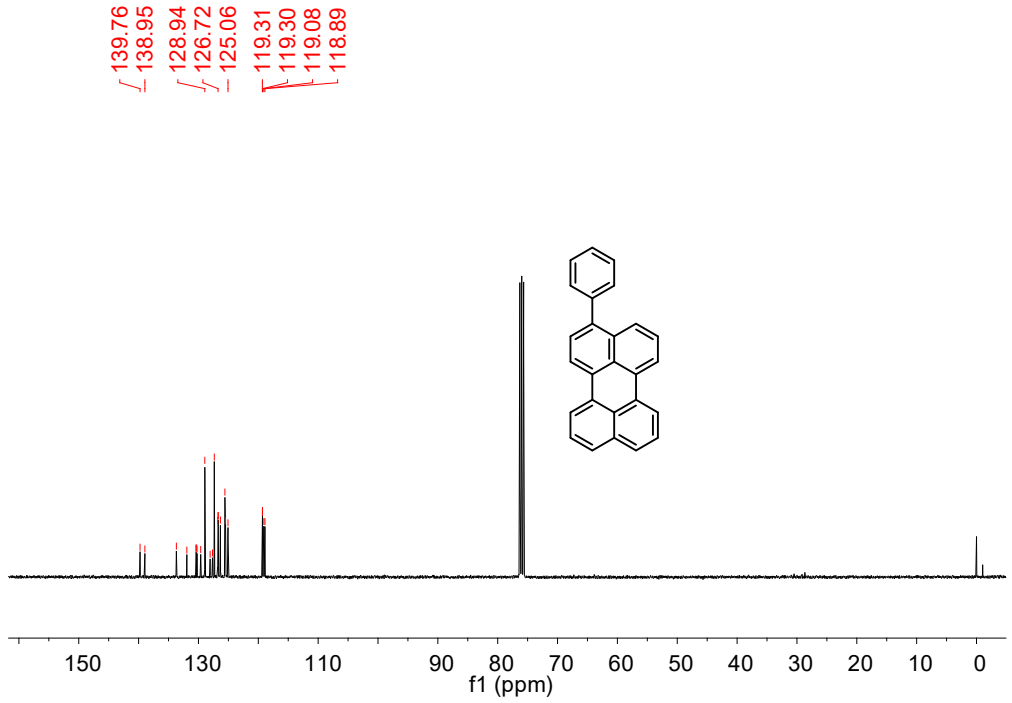

Figure. S17. ^{13}C NMR of **PY-Ph** ($CDCl_3$, 100 MHz).

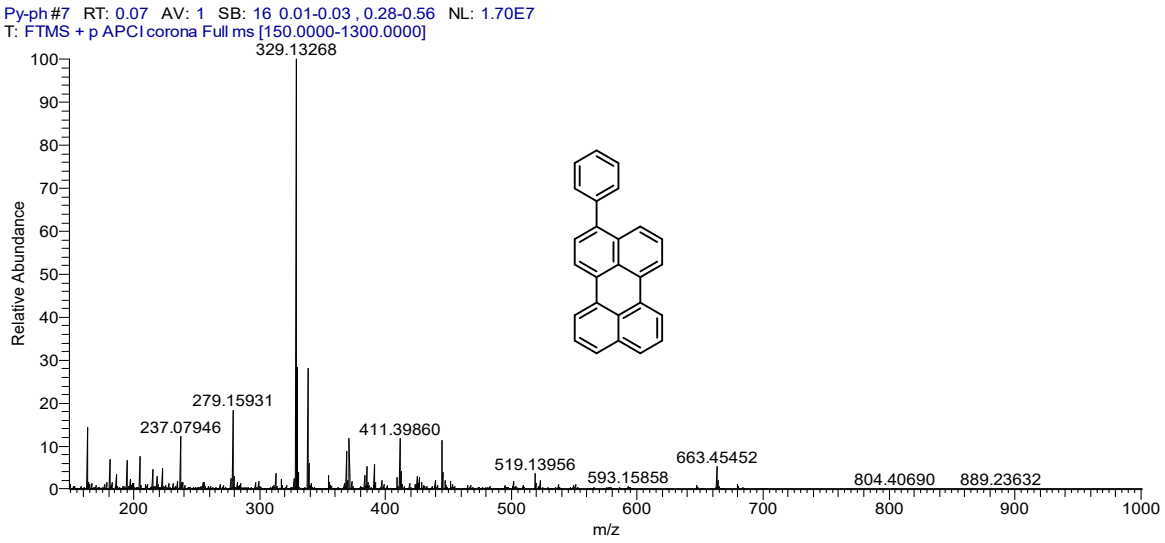

Figure. S18. HRMS of **PY-Ph**.

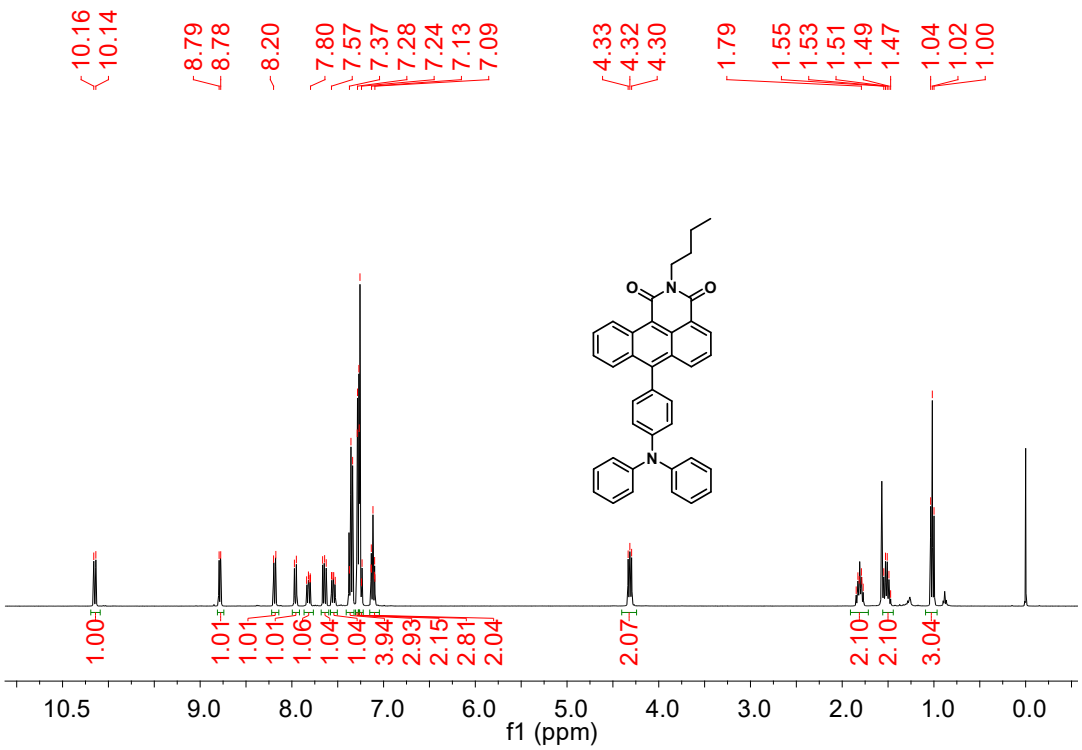

Figure. S19. ^{1}H NMR of **TPA-ACI** ($CDCl_3$, 400 MHz).

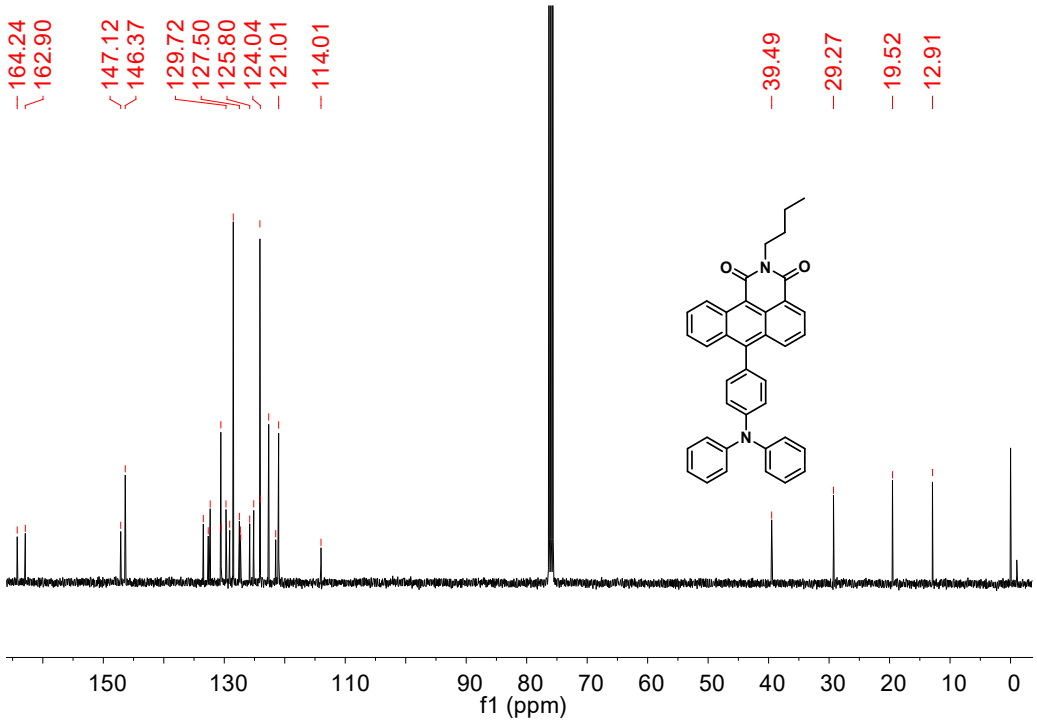

Figure.S20. ^{13}C NMR of **PY-Ph** ($CDCl_3$, 100 MHz).

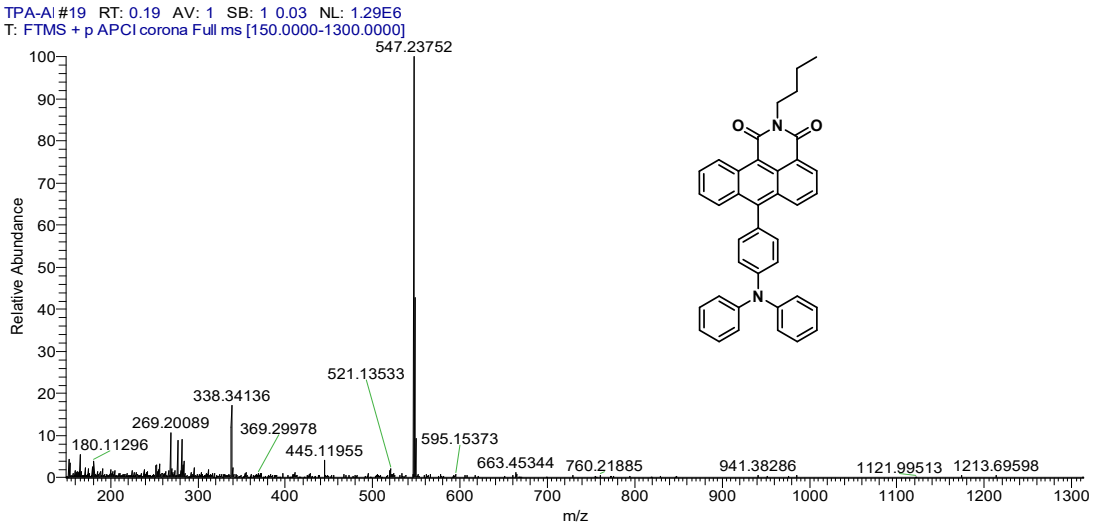

Figure. S21. HRMS of **TPA-ACI**

3. Fluorescence emission spectra

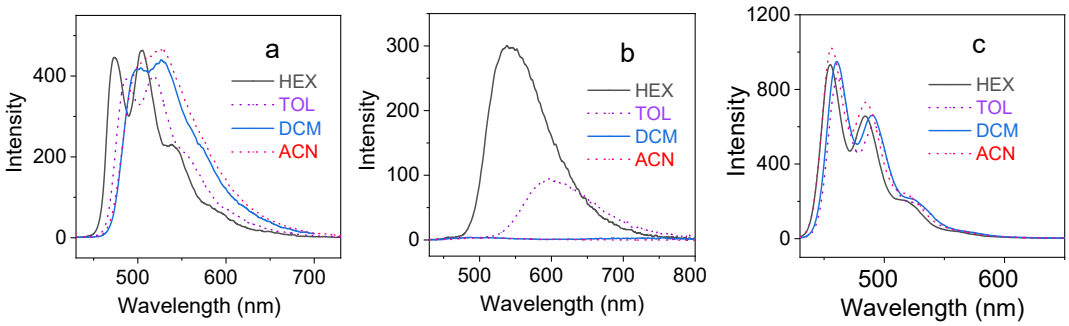

Figure. S22 Fluorescence emission spectra of (a) **Ph-ACI**, (b) **PY-ACI**, (c) **PY-Ph** in different solvents, optically matched solutions were used (A = 0.088). λ_{ex} = 420 nm, 25 °C. "HEX" stands for *n*-hexane, "TOL" stands for toluene, "DCM" stands for dichloromethane and "ACN" stands for acetonitrile.

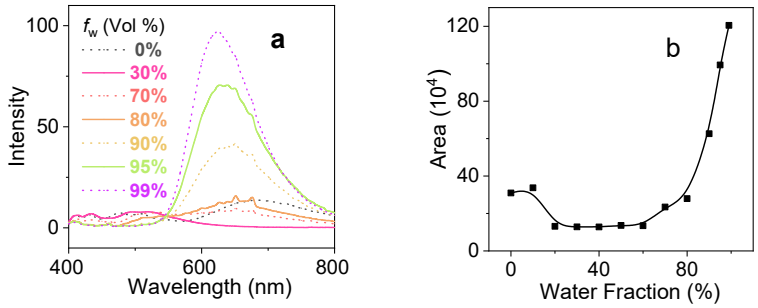

Figure. S23 Fluorescence emission spectra of **TPA-ACI** in THF/water mixtures with different water fractions (f_w). λ_{ex} = 420 nm, 25 °C (b) Integral area of **TPA-ACI** in in THF/water mixtures with different water fractions.

.

4. Fluorescence emission decay curves.

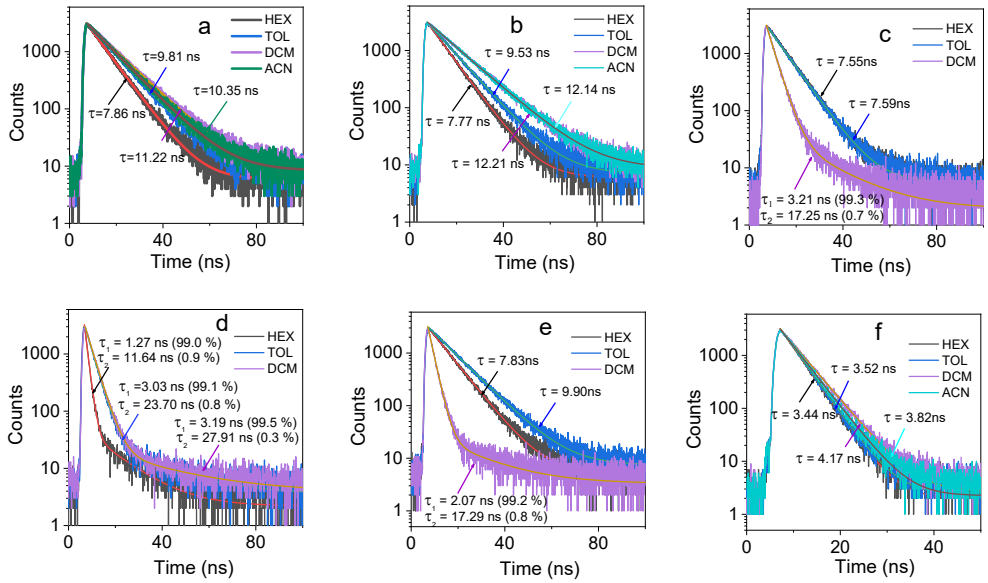

Figure. S24 Fluorescence decay curves of (a) **Ph-ACI**, (b) **NP-ACI**, (c)**AN-ACI**, (d) **TPA-ACI**, (e) **PY-ACI** and (f) **PY-Ph** monitored at emission maxima, λ_{ex} = 441 nm, $c = 1 \times 10^{-5}$ M.

Table. S1 Singlet oxygen quantum yield (Φ_{Δ}) of compounds in different solvents.

	Ph-ACI	NP-ACI	AN-ACI	PY-ACI	TPA-ACI
HEX	12%	16%	20%	19%	–[a]
TOL	11%	13%	59%	77%	–[a]
DCM	3%	8%	99%	60%	–[a]
ACN	–[a]	13%	28%	–[a]	–[a]

"HEX" stands for n-hexane, "TOL" stands for toluene, "DCM" stands for dichloromethane and "ACN" stands for acetonitrile, –[a]: not observed, error：±2.

5. Electrochemical Properties

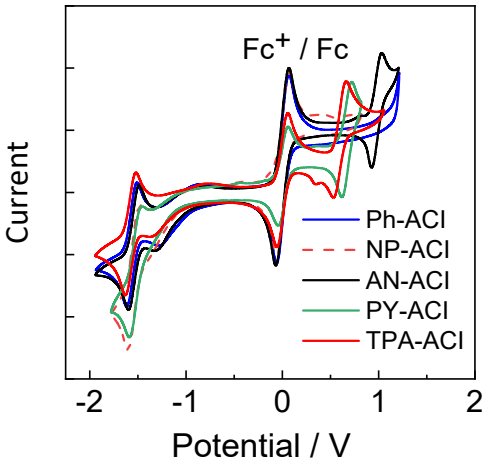

Figure. S25 Cyclic Voltammograms of (a) **Ph-ACI**, (b) **NP-ACI**, (c) **AN-ACI**, (d) **PY-ACI**, and (e) **TPA-ACI** in N_2 saturated DCM containing a $Bu_4N[PF_6]$ (c=0.1 M) supporting electrolyte and $Ag/AgNO_3$ as a reference electrode. Ferrocene (Fc) was used as an internal reference, scan rate:50 mV s^{-1}

$$E_{CS} = e\left[E_{OX} - E_{RED}\right] + \Delta G_S$$

$$\Delta G_S = -\frac{e^2}{4\pi\varepsilon_s\varepsilon_0 R_{CC}} - \frac{e^2}{8\pi\varepsilon_0}\left(\frac{1}{R_D} + \frac{1}{R_A}\right)\left(\frac{1}{\varepsilon_{REF}} - \frac{1}{\varepsilon_S}\right)$$

$$\Delta G^{0}_{CS} = e\left[E_{OX} - E_{RED}\right] - E_{00} + \Delta G_S$$

ΔG^{0}_{CS} is static coulombic energy, E_{OX} and E_{RED} represent the half-wave oxidation potential of the electron donor and the half-wave reduction potential of the electron acceptor, respectively, E_{00} is the energy level at the intersection point of the normalized molecular UV-VIS absorption spectrum and fluorescence emission spectrum, R_{CC} is the distance from the center of the donor to the center of the acceptor calculated by density functional theory (DFT), R_D and R_A represent the radius of the electron donor and electron acceptor in the molecule, respectively. ε represents the static dielectric constant of the solvent.

5. Femtosecond Transient Absorption Spectra

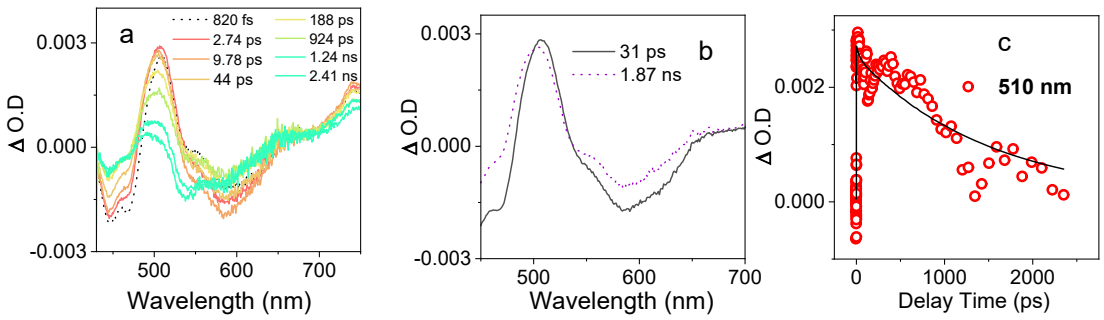

Figure. S26 (a) Femtosecond transient absorption spectra of **Ph-ACI** in DCM, (b) evolution-associated difference spectra (EADS) obtained from global analysis. and (c) kinetic traces at 510 nm, λ_{ex} = 420 nm, 20 °C

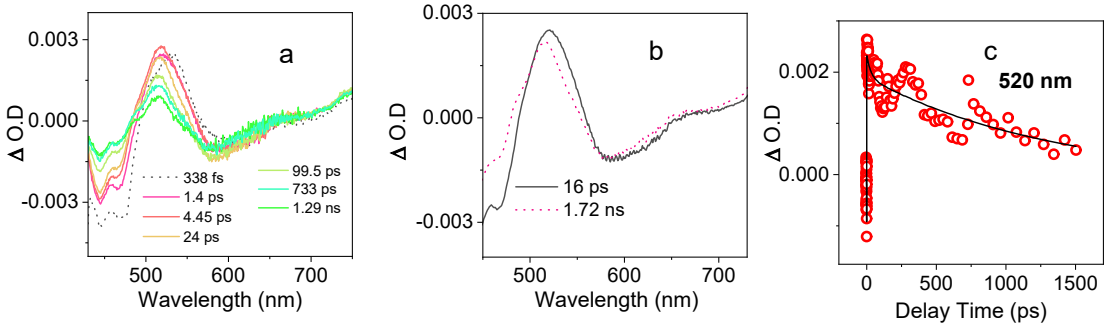

Figure. S27 (a) Femtosecond transient absorption spectra of **NP-ACI** in DCM, (b) EADS obtained from global analysis. and (c) kinetic traces at selected wavelengths, λ_{ex} = 420 nm, 20 °C

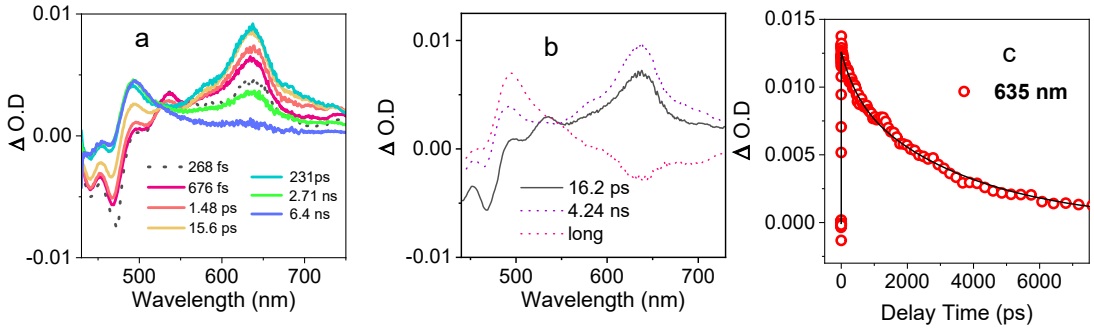

Figure. S28 Femtosecond transient absorption spectra of **AN-ACI** in *n*-HEX, (b) EADS obtained from global analysis. and (c) kinetic traces at selected wavelengths, λ_{ex} = 420 nm, 20 °C

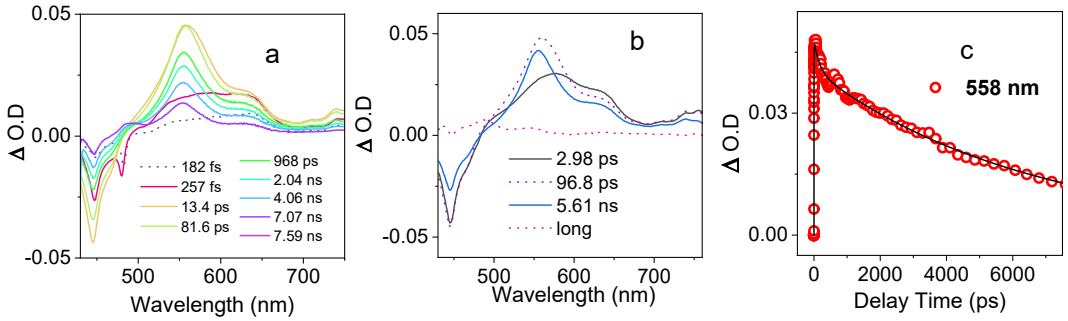

Figure. S29 (a) Femtosecond transient absorption spectra of **PY-ACI** in *n*-HEX, (b) EADS obtained from global analysis. and (c) kinetic traces at selected wavelengths, λ_{ex} = 420 nm, 20 °C

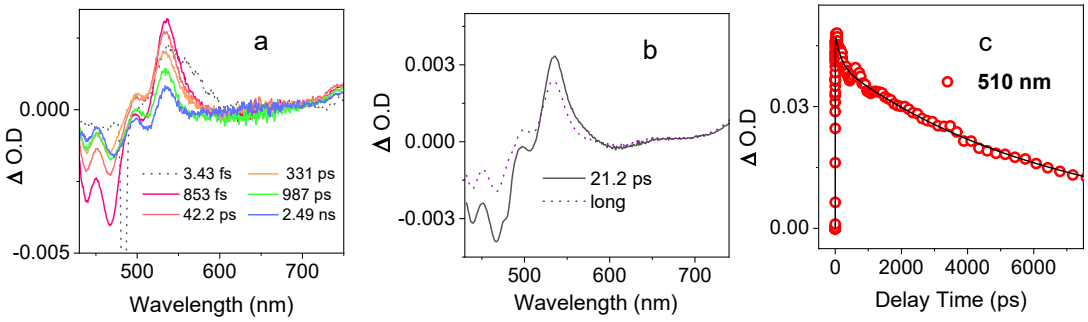

Figure. S30 (a) Femtosecond transient absorption spectra of **NP-ACI** in *n*-HEX, (b) EADS obtained from global analysis. and (c) kinetic traces at selected wavelengths, λ_{ex} = 420 nm, 20 °C

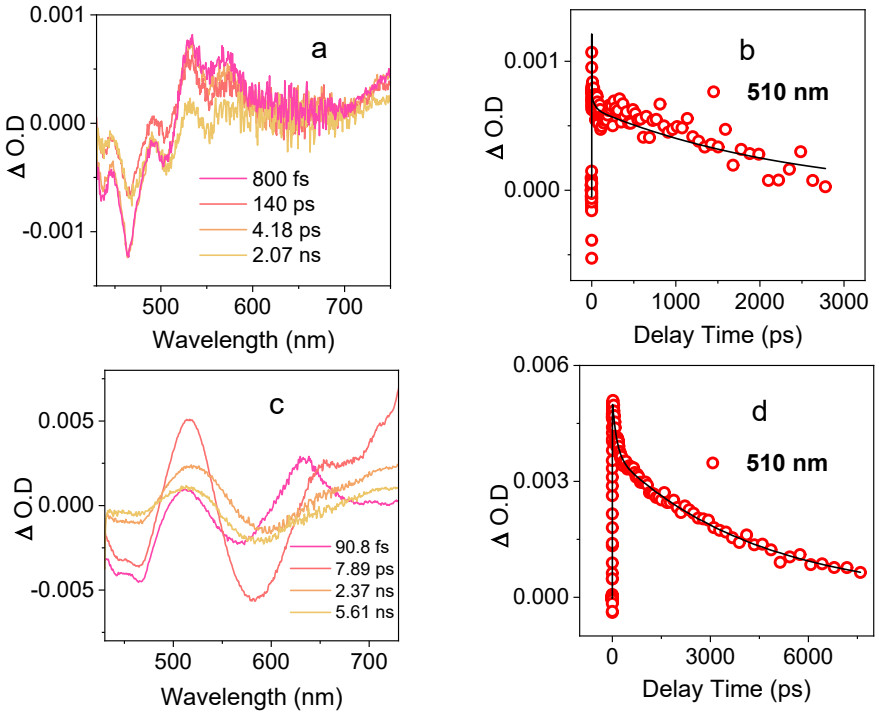

Figure. S31 (a) Femtosecond transient absorption spectra of **Ph-ACI** in *n*-HEX, (b) kinetic traces at selected wavelengths. (c) Femtosecond transient absorption spectra of **TPA-ACI** in HEX, (d) kinetic traces at selected wavelengths, λ_{ex} = 420 nm, 20 °C

6. Nanosecond Transient Absorption Spectra

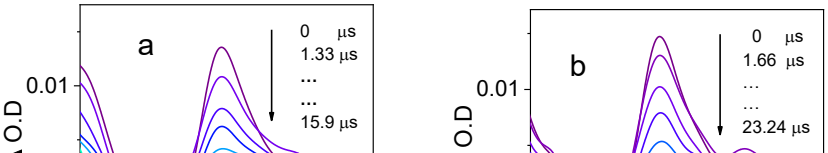

Figure. S32 Nanosecond time-resolved transient absorption spectra of **Ph-ACI** (a), **NP-ACI** (b), **AN-ACI** (c), **PY-ACI** (d) at different time delay. The decay trace of **Ph-ACI** (e), **NP-ACI** (f), **AN-ACI** (g), **PY-ACI** (h) monitored at 490 nm. Conditions: λ_{ex} = 355 nm, 25°C, in *n*-HEX.

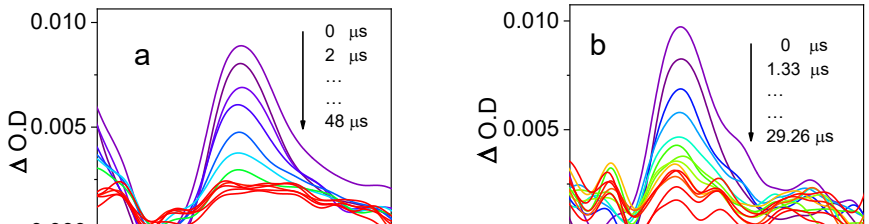

Figure. S33 Nanosecond time-resolved transient absorption spectra of **Ph-ACI** (a), **NP-ACI** (b), **AN-ACI** (c), **PY-ACI** (d) at different time delay. The decay trace of **Ph-ACI** (e), **NP-ACI** (f), **AN-ACI** (g), **PY-ACI** (h) monitored at 500 nm. Conditions: λ_{ex} = 355 nm, 25°C, in TOL.

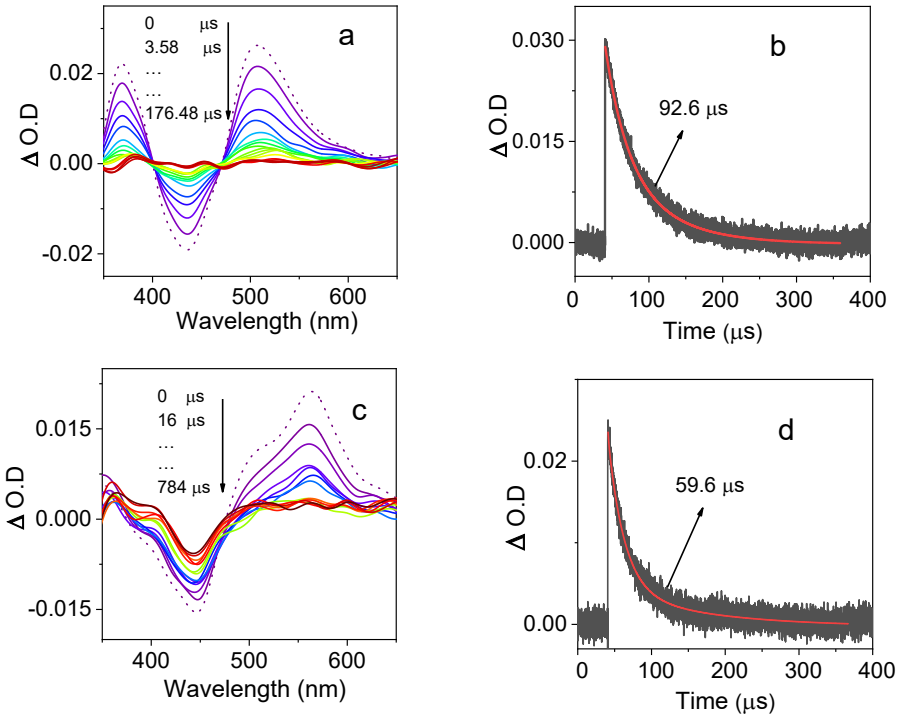

Figure. S34 Nanosecond time-resolved transient absorption spectra of **AN-ACI** (a), **PY-ACI** (c) at different time delays. The decay trace of **AN-ACI** (b), **PY-ACI** (d) detected at 500 nm. Conditions: λ_{ex} = 355 nm, 25°C, in DCM.

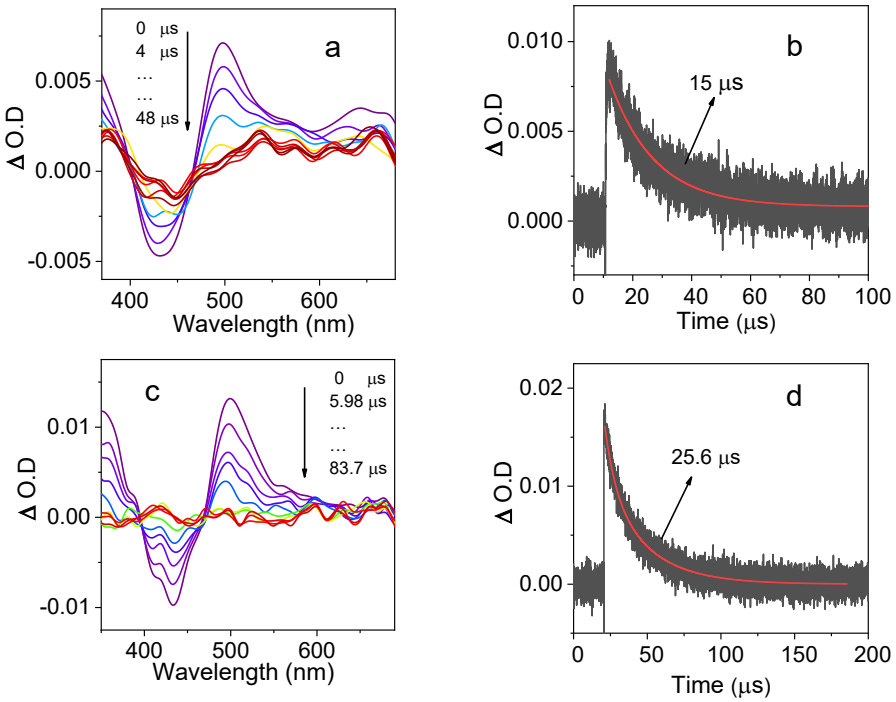

Figure. S35 Nanosecond time-resolved transient absorption spectra of **NP-ACI** (a) and **AN-ACI** (c) at different time delay. The decay trace of **AN-ACI** (b) recorded at 500 nm. Conditions: λ_{ex} = 355 nm, 25°C, in ACN.

8. Density Function Theory Calculations

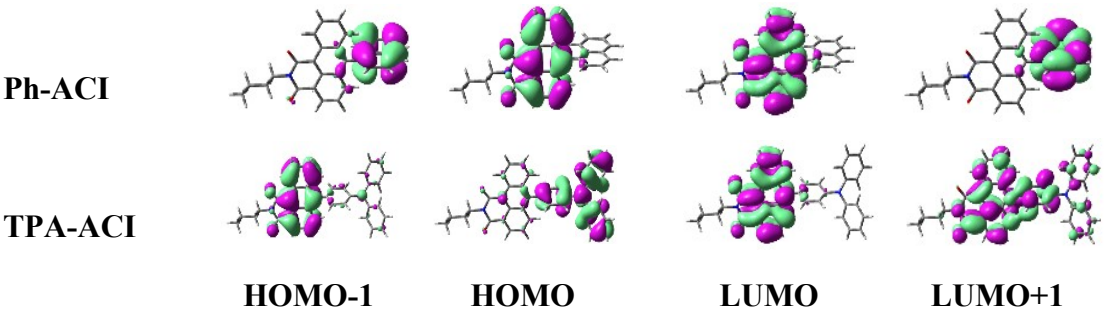

Fig. S36 Selected frontier molecular orbitals of dyes calculated at the DFT (B3LYP/6-31G(d)) level with Gaussian 09W

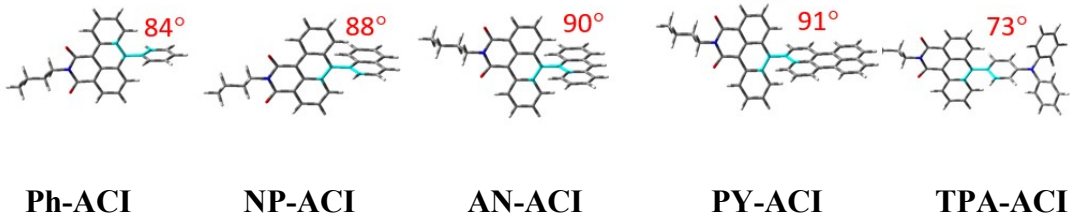

Fig. S37 Optimized ground state conformations and the dihedral angles between the electron donor and acceptor of the dyads. Calculated at the DFT (B3LYP/6-31G(d)) level with Gaussian 09W.

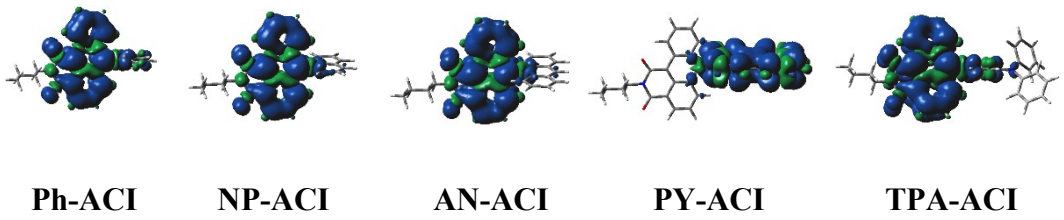

Figure. S38 Spin density surfaces of the triplet state of the compounds at the optimized triplet state geometry. Calculated at the wb97xd/6-31G(d) level with Gaussian 09W.

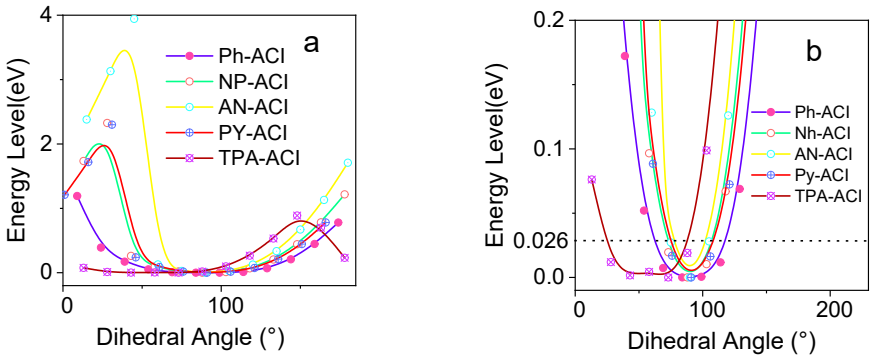

Figure. S39 (a) Potential energy surface (PES) curves of dyads were calculated at the DFT (B3LYP/6-31G(d)) level with Gaussian 09W. (b) Enlarged view of the PES curves near the minima.

Scheme. S1. Simplified Jablonski Diagram Illustrating the Photophysical Processes with Compounds

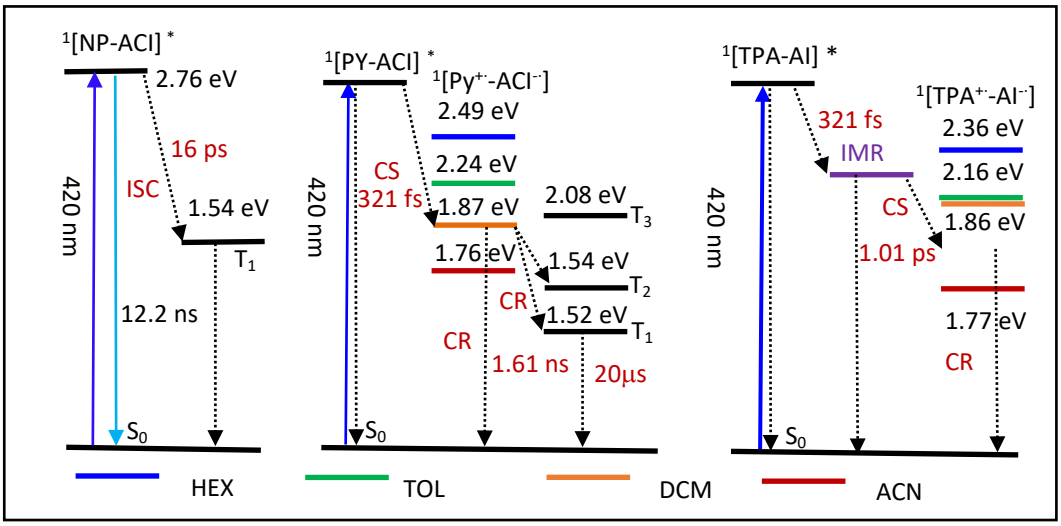

The energy level of CSS, and triplet excited state are derived electrochemical studious, and DFT calculations, respectively.

9. Cell Viability

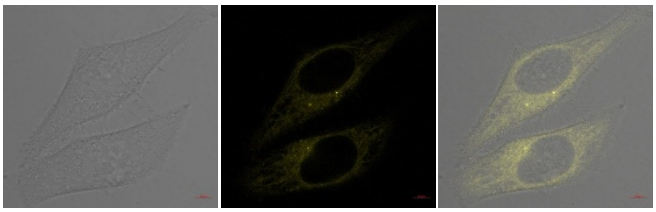

Figure. S40 Bioimaging picture of the Hela cell after incubation for 1 hour with photosensitizer (**AN-ACI**, 1 μg mL^{-1}), λ_{ex} = 480 nm.

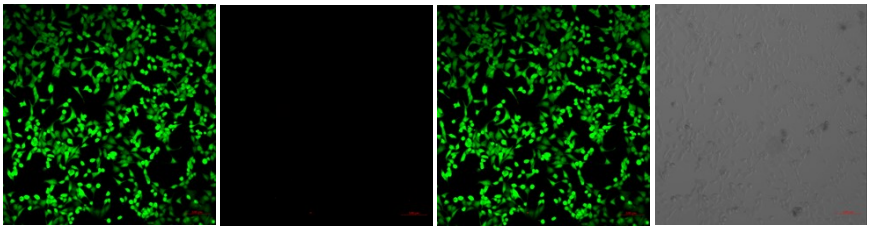

Figure. S41 Live/dead cell co-staining assay of blank by using calcein-AM with green fluorescence for live cells and PI with red fluorescence for dead cells upon white light irradiation of 20 mW cm^{-2} for 5 min. For calcein-AM, the excitation was 488 nm, and the emission filter was 490~540 nm; For PI, the excitation was 543 nm, and the emission filter was 590~680 nm.

10. References

1. H. Langhals, G. Schonmann and K. Polborn, *Chemistry*, 2008, **14**, 5290-5303.
2. Z. Gao, B. Han, K. Chen, J. Sun and X. Hou, *Chem. Commun.*, 2017, **53**, 6231-6234.
3. J. Xu, G. Niu, X. Wei, M. Lan, L. Zeng, J. M. Kinsella and R. Sheng, *Dyes Pigment.*, 2017, **139**, 166-173.